Proceedings of Lunar and Planetary Science, Volume 22, pp. 185-193
Lunar and Planetary Institute, Houston, 1992

Impact Cratering from LDEF's 5.75-year Exposure: Decoding of the Interplanetary and Earth-Orbital Populations

J. A. M. McDonnell and the Canterbury LDEF MAP Team

Unit for Space Sciences, University of Kent at Canterbury, Kent CT2 7NR, United Kingdom

The LDEF multiple-foil microabrasion experiment (MAP) was exposed in five pointing directions stabilized relative to the orbit motion vector. Penetration records from this exposure provide an excellent opportunity for the decoding of the possible contribution from Earth orbital (bound) components and hyperbolic (unbound) particulates of extraterrestrial origin. Complemented by other experimental data at larger dimensions on LDEF, a preliminary flux distribution is derived for the nominal east- (ram), west- (trailing), and space-pointing detector surfaces. Modeling of the orbital dynamics for these two classes of population, and their collisional probabilities with LDEF's near-circular orbit, demonstrates a high anisotropy in the flux rate for the different detector locations. Bound and unbound particulates are also seen to have quite different signatures regarding anisotropy. According to the modeling, the west- and space-pointing flux distributions must dominantly represent the unbound extraterrestrial populations. The different impact velocities on these two faces also permits, with computer modeling, the derivation of the average geocentric particle impact velocity; an extension of the same modeling permits, further, a transformation to predict the flux distribution of the same unbound particulates on the east face. Hence we can identify any excess flux observed on the east face as a possible component in Earth orbit. The east-to-west flux ratio for the MAP data is 34 ± 7 for the penetration of aluminum at 5 μm and 7.3 ± 1.7 at 30 μm; the space-to-west ratio is 4.9 ± 1.0 at 5 μm (Niblett, 1991). These data demonstrate, using the modeling developed and that of Zook (1991), that LDEF impacts on all detectors are dominated by unbound and hence extraterrestrial particulates above particulate masses of 6.4×10^{-10} g mass. However, for small particulates an orbital component is clearly identified on the east and side (N,S) faces that exceeds the interplanetary flux distribution by a factor of around 4 on the east face. The source is not yet identified, but the possible role of space debris and aerocaptured natural interplanetary dust is discussed. The data are compared to craters reported on the Solar Maximum Mission (SMM) louvres (Laurence and Brownlee, 1986). The SMM data are consistent with LDEF MAP data as a crater distribution, but very significant revisions to the interpretation of the SMM data are identified. The application of a new dimensionally scaled penetration formula, incorporating hypervelocity impact calibration to 16 km s^{-1} velocity, shows that the interplanetary component measured on the LDEF foils is consistent with interplanetary sources measured at 1 AU heliocentric distance.

LDEF's EXPOSURE OPORTUNITY

LDEF's delayed launch, and the extension of its mission to nearly six years, now provides us with a unique opportunity for studying the near-Earth space environment. Its role of environmental assessment and space system evaluation extends over a very wide range of disciplines. We focus here on the particulate environment, in particular the role played by Meteoroid Principal Investigator (PI) experiments (Ref. NASA SP-473) and the Meteoroid and Debris Special Investigator Group (M-D SIG) data. Exposure factors relevant to LDEF's orbital and impact exposure have been published (*McDonnell et al.*, 1990, 1991a,b). Essential characteristics are exposure time = $1.822.10^8$ s; mean altitude = 458 km; orbital velocity (at mean altitude) V_L = 7.64 km s^{-1}; orbital inclination i_L = 28.5°. PI experiments of special interest in defining the average distribution of impacts on the detector surfaces are listed in Table 1.

Detectors are generally dispersed over the 14 pointing directions, 12 of which are peripheral in 30° steps (Fig. 2, inset) together with the space (SP) and Earth (E) faces. An exception is the M-G SIG tray and clamp survey data where 24 peripheral directions are available from LDEF tray edges and clamps, even though each surface is accessible to impact from a solid angle of almost 2π steradians. LDEF's performance during exposure as a geocentrically stabilized platform appears excellent, although an offset of some 8° relative to the nominally east-pointing face was evident (*LDEF Newsletter*, April 1991). Its attitude stabilization offers a statistically "stationary" exposure geometry to bound orbits; because of fairly rapid

TABLE 1. Key experiments on LDEF used to define the particulate penetration and impact distribution (*LDEF Experimenters Handbook*, NASA SP-473).

Experiment Acronym	LDEF AO Reference	Nature of Detector	Sensitivity (Critical Dimension)
MAP	023	Aluminum and brass foils; and aluminum	1.5 μm - 30 μm + 1 mm
IDE	201	Silicon solid state detection	0.5 μm, 1.0 μm
Frecopa	138	Aluminum foils	>0.75 μm
SDIE	0001	Aluminum plates	microscopy limit
UHCRE	178	Teflon (FEP) + Chemglaze	120 μm + 80 μm

orbit precession, however, it constantly sweeps through a wide range of heliocentric directions that range from ecliptic inclinations of $\pm(i_L + i_E) = \pm 51°$ where i_E is the Earth's polar declination. We see therefore, together with a 360° ecliptic longitude exposure, a very broad range of sampling of interplanetary particulates. With their hyperbolic velocity they have accessibility, albeit anisotropically, to all LDEF faces. For orbital particulates access is even more restricted, and extremely high eccentricities would be required to strike the space or east faces. Hence the anisotropy of LDEF flux distributions provides a powerful tool for analysis of the contribution from the two categories of dust, examined and delineated only at this stage of analysis by characteristics of their orbital parameters. From the velocity inferred from the data, we are able to make an important distinction between "bound" and "unbound" particulates in geocentric space. We will later wish to draw from other sources of knowledge concerning the origin of the particulates, such as the chemistry of residues.

IMPACT AND PENETRATION DATA

Data from experiments (listed in Table 1 and others) are plotted in Fig. 1, referred to the flux of particulates penetrating a given thickness of aluminum. Where thick target data are used (namely the nonperforation of a semi-infinite target) an equivalent thickness of foil for the ballistic limit (f_{max}) is found by using f_{max} = crater depth (P_C) × 1.15 based on micrometer dimension thin foil hypervelocity impact data (*McDonnell,* 1970); other workers (e.g., *Humes,* 1991) have suggested $f_{max} = 1.5$ to $1.7 \times D_c$. The ballistic limit is defined as the maximum thickness of target that is just perforated. Where crater depth is not available and yet crater diameters are, we take an average crater diameter-to-depth ratio (D_C/T_c) based on LDEF studies that show a narrow distribution centered at $(D_C/T_c) = 0.59 \pm 0.15$ from an east-facing LDEF aluminum clamp study (P. J. Newman, personal communication, 1991). Similar ratios have been found by D. E. Brownlee and F. Hörz (personal communication, 1990). Hence we take $f_{max} = 0.59 \times 1.15\ D_C = 0.68\ D_C$ for aluminum targets. Comparison of the LDEF thin foil and thick target data will later enable such relationships to be established empirically and with considerably greater reliability.

The multiple foil microabrasion package experiment MAP A0023 consists of many different thicknesses of foil, mostly aluminum but also brass (in order to chemically discriminate against aluminum oxide debris). Although the penetration crater size distribution will later enable the mass of size distribution to be determined for each foil, currently we plot the data in terms of the cumulative number of penetrations exceeding the (detectable) limit f_{max}. Each flux point Φ plotted in Fig. 1 represents an independent exposure area on the top aluminum foils of MAP. Because of the independence of each point, we can find examples of an apparently positive cumulative slope; this results, however, only from statistical errors in the flux distribution, and a best fit through such data points must be considered weighted by the significance of each measurement.

Data defining the peripheral variation in the flux distribution show a maximum near face 9 (E) but in some instances are exceeded marginally by face 10, even though LDEF is offset

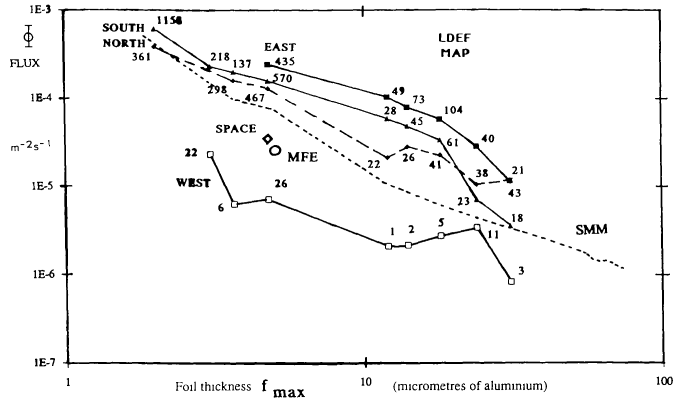

Fig. 1. Penetration data from aluminum foils of the LDEF Micro Abrasion Package (MAP 023). Each point (with perforation counts shown) is derived from independent samples. For comparison, the SMM data are shown representing random orientation exposure directions; it is converted from crater diameter (D_C) to an equivalent foil penetration $f = 0.68D_C$. Asymmetry regarding north and south fluxes is statistically significant, as is the reversal in this bias at $f_{max} = 20\ \mu m$ penetration thickness.

by only 8° toward face 10 relative to face 9. Symmetry of the angular distribution of the flux relative to the orbital motion vector is clearly not upheld by the LDEF data and, interestingly, both the MAP experiments and IDE experiment (*Singer et al.*, 1990) data show this asymmetry to be a function of size. For penetration fluxes at smaller sizes, a bias toward the geographic south direction is evident; for larger (and later shown to comprise dominantly unbound) particulates, the excess is biased toward geographic north and hence toward the ecliptic north. The flux distribution from the space faces is not defined at this stage of analysis over a foil thickness range, i.e., a marginal size distribution is not available since only one thickness of aluminum foil (5 μm) was deployed. The perforation distribution will later be available to derive this. However, the cumulative flux on the space face may be defined very accurately at 5-μm foil thickness from the 193 perforations. MAP data is referred to hard-temper (T6) high-purity rolled aluminum foil measured in thickness for each detector by its mass per unit area on unflown samples to an accuracy of ±2%. Loss by erosion due to atomic oxygen in flight is found to be insignificant for aluminum materials, although its state of oxidation might well have increased during its exposure. The 1.5-μm foils, not analyzed here because of the need to subtract preflight background hole counts, show excellent postflight integrity, hence confirming the stability of the 5-μm foils.

Also shown are preliminary data from experiment AO 178, the UHCRE Teflon cosmic ray experiment covers (*O'Sullivan et al.,* 1984) scanned at Canterbury. The penetration limit for Teflon is currently converted to an equivalent thickness of aluminum target by scaling of target density (ρT) and strength (σT) according to conversion factor of f_{max} (Teflon) = f_{max} (aluminum) × 1.5.

This conversion is based on a study of hypervelocity impacts on differing (but mainly metallic) target materials using iron

projectiles where a functional dependence is found by multivariate minimization technique (*McDonnell and Sullivan,* 1991) of the form

$$f_{max_{Te}} = \left[\frac{\rho A1}{\rho Te}\right]^{0.476}\left[\frac{\sigma A1}{\sigma Te}\right]^{0.134} f_{max_{A1}} \quad (1)$$

Other relationships have been established, based at centimeter dimension impacts into thick targets (*Summers,* 1959)

$$P_c/d_p = 2.25\left(\frac{\rho p}{\rho T}\right)^{0.667}\left(\frac{V}{C_T}\right)^{0.667} \quad (2)$$

where V is the impact velocity and C_T the velocity of sound in the target (which incorporates the strength parameter).

Thin plate relationships (*Fish and Summers,* 1965) have also been established. *Pailer and Grün* (1980) later demonstrate a dependence on the form

$$f_{max}/d_p = 0.772\, d_p^{0.21}\, \epsilon^{-0.06} \cdot \rho_p^{0.73}\, \rho_T^{-0.5}(V\cos\alpha)^{0.88} \quad (3)$$

where ϵ is the target ductility and α the impact angle relative to the normal. This leads to a factor of $f_{max_{Te}} = f_{max_{AL}} \times 1.6$ and is the same factor as that calculated by the Fish-Summers equation.

Before transforming each data point to particulate sizes, a nominal flux distribution is derived for the three critical pointing directions, namely west-, east-, and space-pointing fluxes. The ratio of these distributions is used to compare with the results of our modeling of the dynamics of the LDEF exposure and particulates in geocentric space, termed "dynamic modeling." Hence we can begin on statistical grounds to argue the case for the separation of sources into bound and unbound orbits. At this stage the flux distributions are established by assessing best estimates from the wider dataset available corresponding broadly to the (typically minimum and maximum) fluxes for the west and east faces. The small contribution of the 8° LDEF offset is not accounted for at this stage. We will later wish to revisit this area when more data are available, noting that the east face 9 is not always the maximum peripheral flux nor is the west face 3 the minimum value. Again, LDEF's opportunity for the experimental establishment of the effect of this offset and factors such as dimensional scaling will be a valuable asset at a later date.

PENETRATION MODELS DEDUCED FROM LDEF

Rather than apply calibration formulae to reduce penetration data to particulate mass, at this stage we need only invoke the functional dependence of the penetration equations to compare the relative anisotropy. From the LDEF dataset shown in Figs. 1 and 2 we are able to derive a coherent model for the east and west faces varying from $f_{max} = 1.5$ to $f_{max} = 1000$ μm equivalent aluminum foil thickness, and at 5 μm a well-defined space flux point (MAP experiment) corresponding to 193 impacts. The distributions are shown in Fig. 3. Though these distributions will later be refined as more data are made available, they already lead to some very significant inferences. If we could remove the effects of LDEF's orbital motion from this dataset, we would be in a position to compare the deduced fluxes to other surveys of the terrestrial meteoroid environment (e.g., *Cour-Palais,* 1969); for comparison to interplanetary flux assessments (e.g., *Grün et al.,* 1985) we would also have to incorporate gravitational enhancement and Earth shielding. First, however, we must begin to understand the flux anisotropy before we can transform to particulate diameter mass.

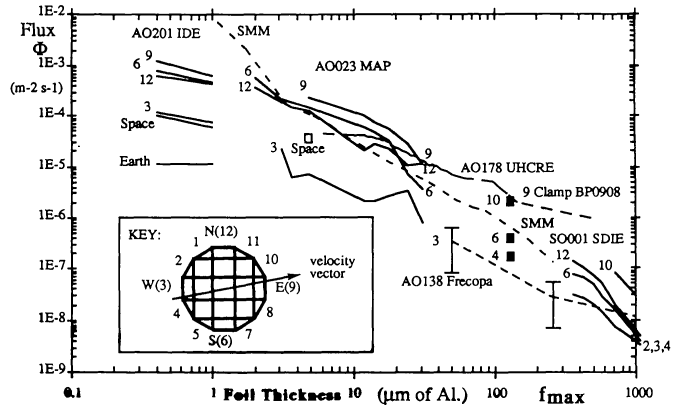

Fig. 2. Penetration and semi-infinite target data from a wider set of LDEF data, including that of the SDIE experiment (*Humes,* 1991), the UHCRE experiment [teflon covers (*O'Sullivan,* 1984) analyzed at Canterbury], the FRECOPA experiment (*Mandeville,* 1990), and the high-sensitivity IDE experiment (*Singer et al.,* 1990). Data are referenced to the equivalent thickness of aluminum foil.

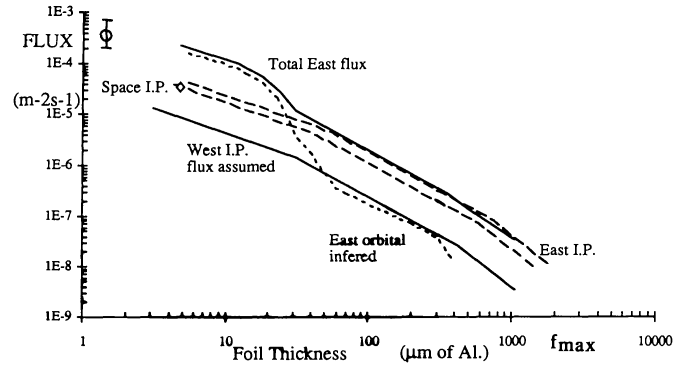

Fig. 3. Flux data summarizing the east-, west-, and space-pointing flux distribution shown (as solid lines) from LDEF impact experiments (in Fig. 2). Also shown is how the west flux transforms to an expected east flux using the modeling described. This compares well with the observed flux for $f_{max} > 30$ μm and supports the extraterrestrial origin of those particulates. Below this foil thickness ($f_{max} > 30$ μm) the excess flux on the east (and supported by the north and south fluxes relative to the space flux) shows a dominance by orbital particulates. These Earth-orbital particulates are not able to reach the west or space faces unless the orbits are of high eccentricity (e.g., GTO orbits).

MODELING OF THE PARTICULATE ENVIRONMENT

Realization that LDEF's vast dataset would never enable discrete analysis and identification of the particular properties of each impacting projectile, statistical models have been developed to represent both possible populations in orbit and unbound particulates. We focus here on the three-dimensional model for the unbound populations that (because of LDEF's precession) permits LDEF to orbit through what is essentially an isotropic, but geocentrically referenced, population. Principles of the computer model are based on the transformation of a three-dimensional distribution of particulates at a velocity V_{PE} to a detector of velocity V_L. These particles (in the absence of Earth shielding) would strike a stationary detector ($V_L = O$) equally on all faces and at a constant velocity. The normal component of this velocity is taken to determine the average penetration efficiency for a flat detector, and will be lower than the approach velocity, typically by some 35%; the value is dependent upon Earth shielding factors. The detector (LDEF) is then moved (V_L finite) relative to this distribution and each particle velocity vectorially added to the detector to calculate new angles of incidence, impact velocity, and the frequency of encounter. Further details have been published (*McDonnell et al.,* 1991b). Any detector surface on LDEF can be simulated; the simulation uses the normally resolved impact velocity in line with numerous penetration experiments and Zook's modeling (*Zook,* 1991). Velocity is a free parameter and, by varying the modeling to best fit the data, the velocity may be inferred.

This so-termed "dynamic modeling" is applied initially to compare with the LDEF MAP fluxes at f_{max} for the 5-μm west and space data; this yields a value of the geocentric particle velocity of $V_{PE} = 17.4 \pm 2$ km s^{-1} leading to a velocity at infinity relative to the Earth of $V_\infty = 13.6 \pm 2$ km s^{-1}. The same modeling is then extended (from the same west population) to predict the east unbound flux. This enhancement on the different faces is due to two factors: (1) a higher impact velocity due to the detector's motion, termed a sensitivity enhancement, and (2) a collisional frequency enhancement at the same mass (*McDonnell et al.*, 1991a,b). *Zook* (1991) incorporates similar concepts and demonstrates meteoroid population east-west enhancements at constant crater size. This comparison of penetration or cratering of fluxes can be performed using as dominant parameters only the slope of the size distribution and the exponent of the velocity dependence β of the cratering efficiency, e.g., of the form $f_{max} = KV^\beta$ where V is the normal component of the impact velocity. Results for the east-facing meteoroid flux predicted by our modeling (*Sullivan,* 1991) based on the west flux are seen (Fig. 3) to be in surprising agreement with the observed east flux at larger dimensions. The prediction is notably divergent, however, at the smaller size of particulates. Clearly something differs for the micrometer-dimension particles, which we address below; for the thicker foils, however, we see that extraterrestrial particulates must dominate by virtue of the high velocity demanded, even though chemical arguments for particulate origin are not yet able to support the physical arguments. We identify below quantitative differences between the modeling of Zook and Sullivan; however, both analyses support, by examination of measured space-to-west ratios, velocities well in excess of bound particulates for the medium and large masses hitting LDEF. The deduced velocity from our modeling agrees well with established meteoroid trail analysis (*Southworth and Sekanina,* 1973) but using Zook's analysis, velocities would be higher (Figs. 7 and 8).

Though the application of this dynamic modeling must be backed up by further observational data on LDEF and differences in the modeling (see below) must be resolved, the extraterrestrial origin of the majority of impacts on LDEF is clearly a "necessary" and probably largely "sufficient" condition except at the smaller masses. With knowledge of the penetration velocity and perforation distribution, we can examine how to transform to a particulate mass distribution. We must return later to issues concerning modeling, but first we need to involve appropriate penetration relationships and, in particular, examine those used to decode the Solar Maximum Mission (SMM) impact cratering data.

HYPERVELOCITY IMPACT PERFORATION AND CRATERING CALIBRATION

Data analyzed here comprise the resultant crater dimensions (e.g., either diameter D_c or depth P_c) or for thin targets the thin plate penetration thickness f_{max}. Based on widely observed constancy of the ratio between crater volume and particle kinetic energy we can say that for a given type of projectile and target, the ratio of target dimension to projectile diameter will be constant. Thus, for example, the ratio D_c/d_p or f_{max}/d_p is only weakly dependent upon the value of d_p. In practice a slight dimension scaling effect will be introduced; typically this might be for a process that depends upon, for example, area-to-mass of a projectile (as in the ionization yield) or upon the velocity gradient during cratering (a viscosity term).

The effect of these dimensional effects is to make cratering less efficient at smaller dimensions, but the effect is only weak because of the dominance of the fluid flow "hypervelocity" phases. We may still express penetration relationships in the form

$$D_c/d_p = K\, f(V_p^\alpha, \rho_p^\beta, \rho_T^\gamma, \sigma_T^\delta).\, d_p^s \qquad (4)$$

where $\alpha \sim 2/3$ represents functionally the particle kinetic energy dependence; $\beta \sim 1/3$ and $\gamma \sim 1/3$ represent a one-third power law dependence upon the projectile-to-target-density ratio ρ_p/ρ_T.

Both δ and s are small, reflecting the small influence of target strength and projectile dimension. Denoting the dimensional scaling effect, s is generally ignored (= O) in analyzing data from a set of experiments from just one particular impact facility either (1) because of the narrow range of dimensions involved or (2) because particle dimensions may vary in a deterministic manner with velocity. In an electrostatic accelerator, for example, the particle mass available for calibration is found to be proportional to the inverse fourth power of velocity. In the latter case, such dimensional dependence may become subsumed in the small changes at apparent velocity exponent α.

Considerable data do exist, however, on ballistic impact test (d_p = millimeter to centimeter dimensions) and also at submicrometer dimensions for Van der Graaff accelerators. This wide range of particle diameters is seen to be a vital element in establishing the value of the exponent s. *Pailer and Grün* (1980) surveyed such data and established a functional dependence upon $m_p^{1/14}$, which implies at constant particle density a value of s = 3/14 = 0.21. This dependence we now see to be very strong, by comparison to other estimates (e.g., *Fish and Summers,* 1965; *Nauman,* 1966; *Cour-Palais,* 1969), which led to a value of s = 0.056, namely dependence on the form $d^{1/18}$ or $m^{1/54}$. The effect of scaling for d_p = 1 μm to 1 mm is shown in Figs. 4 and 5 for numerous penetration analyses. In Table 2, we compare the dimensional scaling of *Pailer and Grün* (1980) to that of dimensional scaling exponent of s = 0.056 favored by other workers and that inferred by the comparison of the thin foil hypervelocity calibration data with macroscale data.

We see that over 4 decade magnitudes in particle size (12 magnitudes in mass) the two dimensional dependences differ by a factor of 70 in terms of the projectile mass inferred to cause a crater of a particular dimension.

In considering why the *Pailer and Grün* (1980) formula size dependence is so strong, we should note that it attempted to include within its scope both large and small projectiles, metallic and plastic targets, and a wide range of velocities. The parametric relationship may well have been a fair fit to that

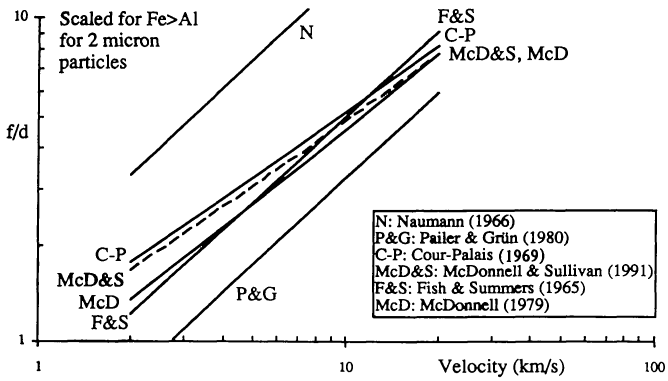

Fig. 4. Penetration ratios defined by the ballistic limit of foil thickness relative to the projectile diameter as a function of velocity for numerous formulations (key) and referred to projectile diameter of d_p = 2 μm. Differences are largely explained by the dimensional scaling beyond calibration regions.

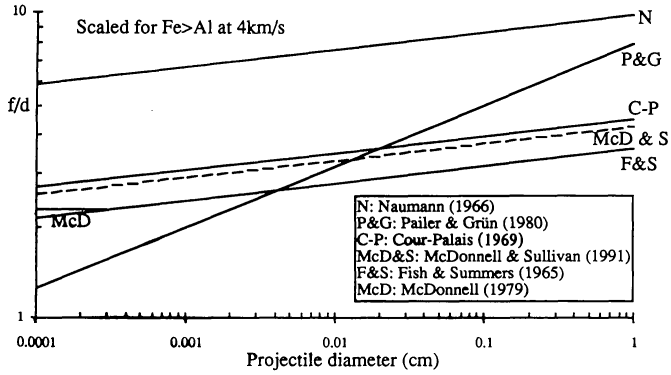

Fig. 5. Penetration ratios at a constant velocity (4 km s^{-1}) shown as a function of projectile diameter d_p. As in Fig. 4, dimensional scaling dominates the divergence of the *Pailer and Grün* (1980) formula.

wider dataset, but it resulted (due to the limited nature and serendipitous bias of the data available) in the "forcing" of the dimensional dependence exponent to an unacceptably high value. We have in the newly scaled foil perforation equation of *McDonnell and Sullivan* (1991) taken a more restricted approach where similar projectile and target conditions are compared at the same velocity at micrometer and at centimeter scale for metalic targets. At larger dimensions, we take established penetration data of *Summers* (1959) for centimeter-scale projectiles at velocities of up to 6 km s^{-1} on metallic targets; we take at micrometer dimensions an enhanced dataset (*McDonnell,* 1970) for iron projectiles on aluminum foils varying from 0.76 μm to 11 μm, and velocities varying from 1 km s^{-1} to 16 km s^{-1}. In the latter data, ballistic limits were studied and also larger perforations (supramarginal) regions were investigated and extensive calibration reduced absolute errors to <±2%. The dataset must represent a clearly preferred basis for interpreting microparticulates on the LDEF foils and (with minor transformations) microcrater data from semi-infinite targets; this microscale foil data is clearly incompatible with the Pailer and Grün formula.

The equation now used to decode penetration data is given as (*McDonnell and Sullivan,* 1991)

$$f_{max}/d_p = 1.023 . d_p \cdot {}^{0.056}\left(\frac{\rho_p}{\rho_T}\right)^{0.476}\left(\frac{\sigma AL}{\sigma_T}\right)^{0.134} \cdot V_p^{0.664} \quad (5)$$

where d_p is measured in cm and V in km s^{-1}.

TABLE 2. Comparative decoding of particulate mass at widely ranging dimensions using differing dimensional scaling exponents corresponding to s = 0.056 (*Summers,* 1959; *McDonnell and Sullivan,* 1991) and s = 0.021 (*Pailer and Grün,* 1985).

Increase of inferred particle dimension for d_p = 1 mm compared to d_p = 0.1 μm	at s = 0.056 $(10{,}000)^{0.056}$ = 1.67	at s = 0.21 $(10{,}000)^{0.21}$ = 6.92
Corresponding particle mass change due to scaling estimated for given crater Dc/dp ratio and other conditions	4.70	331.1
Comparative discrepancy	1.00 (reference assumed)	70.5

A relative discrepancy of 70 in the projectile mass inferred from a given crater may result for projectile dimensions ranging from 0.1 μm to 1 mm when the two scaling relationships are compared.

It may be compared to the *Pailer and Grün* (1980) relationship (equation (3)) and that of Summers (equation (2)). It differs from the Pailer and Grün formula essentially in the dimension scaling dependence and from the Summers relationship in the incorporation of target strength and our adjustment to fit the microscale data.

Of special significance in the concern for space debris, the SMM data have previously been related to an incident particle mass distribution by the Pailer and Grün formula (*Laurance and Brownlee,* 1986). This, by comparison to other mass distributions, led to the debris-dominated (dirty space) microparticle population. We have seen, however, that the basis for this formula makes it inappropriate for interpretation. Furthermore, in Fig. 4 of *Laurence and Brownlee* (1986), other LEO space penetration data were plotted that were transformed to mass by other penetration data. As an example, the MFE shuttle deployment of 5-μm aluminum foil in 1982 (*McDonnell et al.,* 1984) yields a flux that is 2 decade magnitudes below the flux interpreted from the SMM data. And yet the 1982 exposure of MFE centers on the mean epoch of the 1980-1984 SMM data acquisition! With the benefit of the revised penetration formula, and noting in Figs. 1 and 2 that the SMM source data crater distributions agree very well with the new LDEF data, we can now provide a new interpretation of that data in terms of particulate mass. Figure 6 shows the SMM data in its published and newly interpreted form (namely Laurence and Brownlee data, McDonnell and Sullivan formula) and the same data using the Pailer and Grün formula. We also see that with a dominant east flux in LEO, due to enhancement of the detector sensitivity and increase of impact rate, the "randomly" oriented SMM aluminum louvers should yield a value of some 1/4 of the LDEF east flux. This is indeed in line with LDEF data; we must conclude that the particulate environment in this size regime shows little evidence of significant change over the period 1980 to 1990.

MODEL DISTRIBUTIONS IN LEO AND IN INTERPLANETARY SPACE: ISSUES IDENTIFIED

Our dynamic modeling of the interplanetary component leads to an inferred value of V_{PE} = 17.4 km s^{-1} (±10%) at LDEF's altitude. This must be first compared to results of other modeling. *Olsson Steel* (1990) derives collisional probabilities for LDEF at constant mass, which are generally in line with our modeling at constant mass, but show east-west ratios some 30% higher than our modeling. To incorporate sensitivity enhancement, however, and yield ratios at constant crater size or penetration, we must know the actual size distribution, namely the LDEF dataset. *Zook* (1991) has performed a more comprehensive approach incorporating, as in our modeling, the effect of collisional frequency, impact angle, velocity, and size distribution. Superior in principle to our current modeling, which is a single (but variable) velocity approach, Zook has included the effect of the finite velocity distribution. We plot results from our modeling and that of Zook for the east and west faces in Fig. 7, and also the large-particle LDEF data. It is seen that Zook's modeling predicts, if we look at values corresponding to velocities typical of meteoroid studies, ratios of east-to-west that are higher than those derived for our east and west nominal distributions. An exception is, of course, the smaller particulates, which he has not modeled in bound orbits; we demonstrate that these are "contaminated" by an orbital component on the east, north, and south faces. The ratio of east-to-west at large dimensions will be best determined by data from the SDIE experiment and preliminary values of 20:1 have been reported (*Humes,* 1991). Consideration of a wider dataset (*Niblett,* 1991) leads to a ratio of east to west of 11.0 ± 2.9 incorporating a 9° offset for D_c > 500 μm, and 14.4 ± 3.6 for the ratio of faces 10 to 4. What must be admitted is a quantitative difference in the two

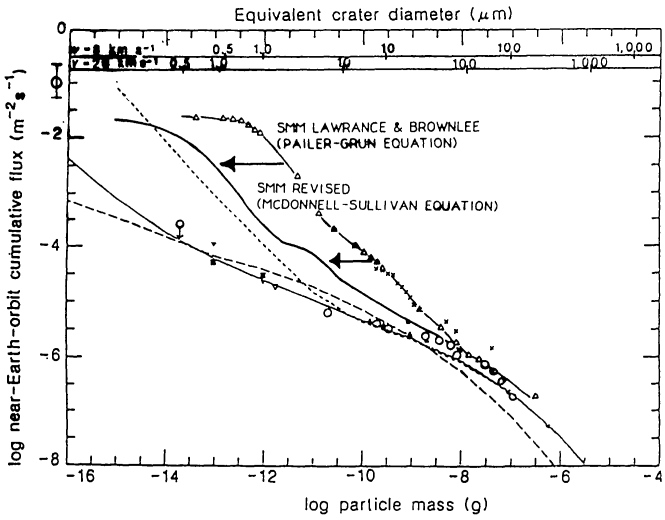

Fig. 6. Spacecraft measurements published by *Laurence and Brownlee* (1986) interpreted by the *Pailer and Grün* (1980) formula (triangles L B P-G) and (using the same velocities) the interpretation using the *McDonnell and Sullivan* (1991) marginal perforation formula L B M-S.

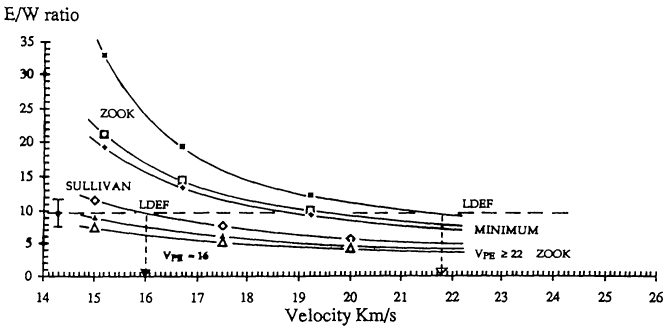

Fig. 7. Interplanetary particulate flux enhancement modeling results applicable to LDEF east and west faces. *Zook* (1991) is shown modeling meteoroid velocity distributions and *Sullivan* (1991) at single velocities. Observed LDEF ratios are shown for foil thicknesses of f_{max} = 287 μm, corresponding to a crater diameter of D_C = 500 μm. The inferred velocities in the two cases are ~16 km s^{-1} (Sullivan) and ≥22 km s^{-1} (Zook) for an east-west ratio of c ~ 10 ± 2 typical of the interim results from the UHCRE thermal covers (Fig. 2). Key: solid squares—Zook, D_c = 500 μm; open squares—Zook, D_c = 100 μm; solid diamonds—Zook, D_c = 2 μm; open diamonds—Sullivan, f_{max} = 287 μm; solid triangles—Sullivan, f_{max} = 57.5 μm; open triangles—Sullivan, f_{max} = 2.3 μm.

modeling approaches for any ratio. We plot also on Fig. 8 the LDEF space-to-west ratio for $f_{max} = 5$ μm, which, from Zook's analysis, would call for a velocity of some 24 km s^{-1}, compared to our value of 17.4 km s^{-1}. Perhaps the discrepancy is modest in terms of a result. Yet, in the converse sense, large changes of the flux ratio result from small changes in velocity. The velocity inferred from applying the two models to the interplanetary (large particle) east-to-west ratio is more divergent. Our analysis (Fig. 7) satisfies the LDEF data at a velocity of some 17.4 ± 2 km s^{-1}; Zook's analysis calls for a higher velocity, perhaps >22 km s^{-1}. Table 3 gives summary data. Refinements of the definition of the data will later be available, which will demand the resolution of the differences between the two modeling approaches. Figure 9 relates the interplanetary components of LDEF data (corrected for Earth shielding and gravitational focusing) to deep space data at 1 AU heliocentric distance.

D. Olsson Steel (personal communication) also points to the selective observational bias in meteor observations, leading to a reducing of the apparent mean meteoroid velocity. It will be interesting to resolve the differences in the two modeling approaches currently so that the particulate velocity can be inferred. Such evidence could well support a revision of the meteor data in line with his data if Zook's modeling is supported in favor of ours.

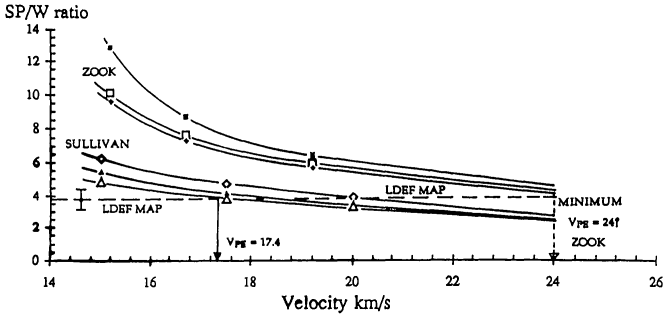

Fig. 8. Interplanetary particule at flux enhancement, modeling results as in Fig. 7, but shown for LDEF's space-to-west ratio. Again LDEF measurements demand a higher velocity from Zook's modeling (>24 km/s^{-1}) compared to that of *Sullivan* (17.4 ± 2 km s^{-1}). Key: solid squares—Zook, D_c = 500 μm; open squares—Zook, D_c = 100 μm; solid diamonds—Zook, D_c = 2 μm; open diamonds—Sullivan, f_{max} = 287 μm; solid triangles—Sullivan, f_{max} = 57.5 μm; open triangles—Sullivan, f_{max} = 2.3 μm.

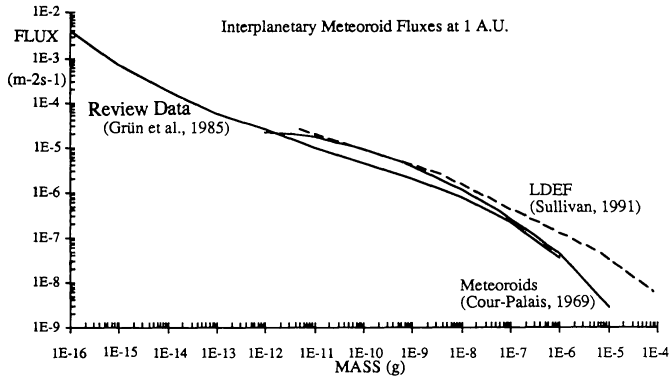

Fig. 9. Reduction of the geocentric referenced particulate flux derived from LDEF data to particulate mass at 1 AU heliocentric distance. The local geocentric velocity of 17.4 ± 2 km s^{-1} transforms to an interplanetary velocity of 13.6 km s^{-1} relative to the Earth. Earth shielding effects are included where relevant for LDEF.

Concerning the origin of the interplanetary particulates, we see that for the larger particulates there is general agreement with the characteristics of meteoroids. These "interplanetaries" do indeed dominate the LDEF surfaces and this prompts the well-discussed question, are they cometary or asteroidal? LDEF may hold the answers, but may need the benefit of chemical evidence to discriminate. Quite certainly impacts are largely from extraterrestrial interplanetary sources in this size range.

As to the small particulate orbital "excess" above the interplanetary component now demonstrated on the east, north, and south faces, we cannot presume until adequate chemical evidence is available that they are exclusively space-age debris. We see no enhancement since the SMM exposure epoch for a start, in what had perhaps been considered an increasingly debris-dominated environment. Our LDEF work now places lower bounds on this enhancement; for the small particulates we have also shown by trajectory calculations (*McDonnell and Ratcliff,* 1991) that aerocapture of the smaller particulates selectively favors capture from interplanetary particulates with low eccentricity and ecliptic inclination. Calculations show the effective altitude for aerocapture (defined as the atmospheric penetration heights for slowing down from an unbound orbit to a high-eccentricity Earth-bound orbit) to be ~215 km at mass 5×10^{-11} g for a value of V_∞ = 5 km s^{-1}. This compares to a lower altitude of ~108 km for mass 10^{-3} g, typical of

TABLE 3. Comparison of LDEF data for space-facing fluxes Φ relative to the north- and south (side)-facing surfaces predicted for interplanetary particulates by *Zook* (1991) and *Sullivan* (1991).

LDEF MAP (at f_{max} = 5 μm) FLUX Φ $m^{-2}s^{-1}$			Zook (calculated)	Sullivan (calculated)
Space/N	Space/S	Space(N+S)	1.40	1.43
0.271	0.222	0.244		
$\Phi_N = 1.26.10^{-4}$	$\Phi_S = 1.54.10^{-4}$	$\Phi_{SP} = 3.42.10^{-5}$	—	—

Modeling parameters: Earth shielding = 0.67 for N,S; 1.00 for space. Particulate velocity = 11.4 km s^{-1} (space), 11.9 km s^{-1} (N,S). Log cumulative mass slope α = -0.34. Velocity exponent of penetration dependence β = 0.66.

TABLE 4. Relative probability for the capture of a particle into orbit (defined as occurring when a particle completes one or more orbit before being absorbed) compared to the total Earth capture cross section (*McDonnell and Ratcliff*, 1991).

V_∞ (km/s)	2.5	5.0	10.0	20.0
Mass = 5×10^{-11} g	8.2×10^{-3}	6.0×10^{-3}	5.3×10^{-4}	2.4×10^{-4}
Capture ceiling* (km)	285	215	188	172
Mass = 10^{-3} g	2.7×10^{-3}	2.0×10^{-3}	2.1×10^{-5}	$<10^{-5}$
Capture ceiling (km)	127	108	105	100

* The capture ceiling is defined as the altitude at which a hyperbolic particle transiting the atmosphere is reduced to a high-eccentricity bound orbit (P. R. Ratcliff and J. A. M. McDonnell, in preparation, 1991).

meteoroid ablation heights. The fraction of particulates aerocaptured is shown in Table 4 for two sample masses and several approach velocities V_∞. Although the aerocapture study does now need appropriate application to the LEO environment, the relative efficiency of the aerocapture of small, slow particulates can be seen in the table. Although significant enough to be able to be detected by LDEF, the lifetime of such captured orbits is short and hence the LEO buildup may be modest. A variant on this process, aerofragmentation capture, supposes that the atmospheric skip leads to fragmentation of larger fragile meteroid agglomerates that release a very high density of subparticles perhaps of micrometer dimensions into orbit. The framentation by electrostatic forces near the Earth has previously been proposed (*Fechtig*, 1976) in a similar attempt to explain the presence of groups and swarms of particles in cislunar space seen by the HEOS II detectors (*Hoffman et al.*, 1975). Both mechanisms are indeed possible and would lead to high concentrations in particular orbit planes at different times. The periodicity observed by the IDE experiment (*Mullholland et al.*, 1991) could well be explained by such natural microparticulates or the result of space missions.

Acknowledgments. The experiment, data, and analysis rationale stems from a wide range of contributions from the experiment team at the Unit for Space Sciences, Canterbury, especially T. Stevenson and K. Sullivan. Alison Rook's and Margaret Fowler's contributions are appreciated in manuscript preparation. The DEF experiment was supported financially by the SERC (U.K.).

REFERENCES

Cour-Palais B. G. (1969) *Meteoroid Environment Model-1969.* NASA SP-8013.

Fechtig H. (1976) *In-situ* records of interplanetary dust particles—methods and results. *Proc. IAU Colloq. 31, Lecture Notes in Physics, 48* (H. Elsasser and H. Fechtig, eds.), p. 143. Springer-Verlag, Berlin.

Fish J. L. and Summers J. L. (1965) *Proc. Hypervelocity Impact Symposium, 7th, 3,* 2.

Grün E., Zook H. A., Fechtig H., and Giese R. H. (1985) Collisional balance of meteoritic complex. *Icarus, 62,* 244-272.

Hoffman H. J., Fechtig H., Grün E., and Kissel J. (1975) Temporal fluctuations on anisotropy in the Earth Moon system. *Planet. Space Sci., 23,* 985-991.

Humes D. H. (1991) Preliminary results of the meteoroid and space debris impact experiment on LDEF. In *Proc. Workshop Hypervelocity Impacts in Space,* Canterbury, United Kingdom, in press.

Laurance M. R. and Brownlee D. E. (1986) The flux of meteoroids and orbital space debris striking satellites in low Earth orbit. *Nature, 323,* 136-138.

Mandeville J. C. (1990) Debris and micrometeoroids: Flight data from Mir and LDEF. *ESA Space Environment Analysis Workshop,* ESTEC.

McDonnell J. A. M. (1970) Factors affecting the choice of foils for penetration experiments in space. *Space Res.*, 314-325.

McDonnell J. A. M. and Ratcliff P. R. (1991) The contribution of interplanetary particles to the near-Earth satellite impact environment: Cometary or asteroidal (abstract). In *The International Conference on Asteroids, Comets, Meteors 1991,* p. 148. Lunar and Planetary Institute, Houston.

McDonnell J. A. M. and Sullivan K. (1991) Hypervelocity impacts on space detectors: Decoding the projectile parameters. In *Proc. Workshop Hypervelocity Impact in Space,* Canterbury, United Kingdom, in press.

McDonnell J. A. M., Carey W. C., and Dixon D. G. (1984) Cosmic dust collection by the capture cell technique on the space shuttle. *Nature, 309,* 237-240.

McDonnell J. A. M., Deshpande S. P., Green S. F., Newman P. J., Paley M. T., Stevenson T. J., and Sullivan K. (1990). First results of particulate impacts and foil perforations on LDEF. *XXVIII COSPAR Meeting,* The Hague, Netherlands, in press.

McDonnell J. A. M., Sullivan K., Stevenson T. J., and Niblett D. H. (1991a) Particulate detection in the near Earth space environment aboard the long duration exposure facility LDEF: Cosmic or terrestrial? *IAU Colloquium No. 126,* in press.

McDonnell J. A. M., Sullivan K., Green S. F., Stevenson T. J., and Niblett D. H. (1991b) Dynamic modeling transformations for the low Earth orbit satellite particulate environment. *IAU Colloquium No. 126,* in press.

Mulholland J. C. (1991) LDEF interplanetary dust experiment: A high time resolution snapshop of the near Earth particulate environment. In *Proc. Workshop Hypervelocity Impacts in Space,* Canterbury, United Kingdom, in press.

Naumann R. J. (1966) *The Near Earth Meteoroid Environment.* NSA TN D-3717.

Niblett D. H. (1991) Survey of flux data derived from impacts on LDEF surfaces. In *Proc. Workshop Hypervelocity Impacts in Space,* Canterbury, United Kingdom, in press.

Olsson Steel D. (1990) Face dependent collision probabilities upon LDEF for heliocentric particle orbits. *XXVIII COSPAR Meeting,* The Hague, Netherlands, in press.

O'Sullivan D., Thompson A., O'Ceallaigh C., Domingo V., and Wenzel K.-P. (1984) *The Long Duration Exposure Facility (LDEF) Mission 1 Experiments, A High Resolution Study of Ultra-heavy Cosmic-Ray Nuclei* (A0178). NASA SP-473.

Pailer N. and Grün E. (1980) The penetration limit of thin films. *Planet. Space Sci., 28,* 231-331.

Singer S. F., Stanley J. E., Kassel P. C., Kinard W. H., Wortmann J. J., Weinberg J. L., Mulholland J. D., Eichorn G., Cook W. J., and Montague N. (1990) First spatio-temporal results from the LDEF Interplantary Dust Experiment. *Adv. Space Res.*, in press.

Southworth R. B. and Sekanina Z. (1973) *Physical and Dynamical Studies of Meteors.* NASA CR-2316.

Sullivan K. (1991) LDEF flux anisotropy: Dynamic modeling and flux transformations to define the interplanetary micrometeroid environment. In *Proc. Workshop Hypervelocity Impacts in Space,* Canterbury, United Kingdom, in press.

Summers J. L. (1959) *Investigations of High Speed Impact Regions of Impact and Impact at Oblique Angles.* NASA TN-D94.

Zook H. A. (1991) Meteoroid directionality on LDEF and asteroidal vs. cometary sources (abstract). In *Lunar and Planetary Science XXII,* pp. 1577-1578. Lunar and Planetary Institute, Houston.